


# Importance of material matching in the calibration of asymmetric flow field-flow fractionation: material specificity and nanoparticle surface coating effects on retention time

Haiou Qu · Ivan R. Quevedo · Sean W. Linder ·  
Andrew Fong · Thilak K. Mudalige 

Received: 9 June 2016 / Accepted: 15 September 2016 / Published online: 3 October 2016  
© Springer Science+Business Media Dordrecht (outside the USA) 2016

**Abstract** Asymmetric flow field-flow fractionation (AF4) coupled with dynamic light scattering or multiangle light scattering detectors is a promising technique for the size-based separation of colloidal particles (nano- and submicron scale) and the online determination of the particle size of the separated fractions in aqueous suspensions. In most cases, the applications of these detectors are problematic due to the material-specific properties of the analyte that results in erroneous calculations, and as an alternative, different nanoparticle size standards are required to properly calibrate the size-based retention in AF4. The availability of nanoparticle size standards in different materials is limited, and this deviation from ideal conditions of retention is mainly due to material-specific and particle coating-specific membrane–particle interactions. Here, we present an experimental method on the applicability of polystyrene

nanoparticles (PS NP) as standard for AF4 calibration and compare with gold nanoparticle (Au NP) standards having different nominal sizes and surface functionalities.

**Keywords** Physicochemical characterization · Asymmetric flow field-flow fractionation · Multiangle light scattering · Nanoparticle standards

## Introduction

With the advancement of nanotechnology, the production and applications of engineered nanoparticles are ever increasing. Nanoparticles are currently used in industrial, biomedical, and consumer products such as foods and dietary supplements (De et al. 2008; Sozer and Kokini 2009). The properties of nanoparticles are different from their bulk counterparts mainly due to their size; therefore, accurate determination of size and size distribution is a crucial part of their physicochemical characterization. Furthermore, the absorption, distribution, metabolism, and excretion of nanoparticles by biological systems are also dependent on their size and their particle size distribution (Chithrani et al. 2006; Lewinski et al. 2008). Multiple methodologies, including dynamic light scattering (DLS), nanoparticle tracking analysis, capillary electrophoresis, electron microscopy, and asymmetric flow field-flow fractionation, are available for the determination of size and size distribution of

---

**Electronic supplementary material** The online version of this article (doi:10.1007/s11051-016-3601-0) contains supplementary material, which is available to authorized users.

---

H. Qu · S. W. Linder · A. Fong · T. K. Mudalige (✉)  
Office of Regulatory Affairs, Arkansas Regional  
Laboratory, U.S. Food and Drug Administration,  
3900 NCTR Road, Jefferson, AR 72079, USA  
e-mail: Thilak.Mudalige@fda.hhs.gov

I. R. Quevedo  
Departamento de Ingeniería y Ciencias Químicas,  
Universidad Iberoamericana, Prolongación Paseo de la  
Reforma 880, 01210 Mexico, Ciudad de México, Mexico

nanoparticles; however, each method has inherent limitations (Lopez-Serrano et al. 2014). For example, dynamic light scattering results are biased towards bigger particles in the suspension (i.e., scattered light intensity is proportional to the diameter to the power of 6), nanoparticle tracking analysis has limitations when detecting smaller nanoparticles ( $\sim <20$  nm) (Gallego-Urrea et al. 2011), and capillary electrophoresis has limitations with the analysis of particles  $\sim 100$  nm and uncharged nanoparticles (Qu et al. 2014).

Even though AF4 has limitations due to membrane fouling, its large dynamic size range of analysis is a distinct advantage over other methodologies (Mudalige et al. 2015c; Ulrich et al. 2012; Wahlund 2013). AF4 uses a narrow ribbon-shaped channel to generate a parabolic flow profile, and particles are separated based on their hydrodynamic diameter. A porous barrier membrane is used to retain the particles in the channel (Mudalige et al. 2015c). Membranes are available in various molecular weight cutoff sizes and are made up of synthetic organic polymers and cellulose acetate.

Various detectors are used downstream of an AF4 system for the quantification of fractions, measurement of sizes, and elemental composition (Mudalige et al. 2015a, 2015b, 2015c). Inductively coupled plasma mass spectrometry is used for the determination and quantification of elemental composition (Mudalige et al. 2015a). DLS and MALS detectors are used for size determination of fractograms (Mitrano et al. 2012). Applications of DLS and MALS, as detectors for size determination in AF4, have been problematic due to multiple factors. For example, these two techniques are unable to produce reliable measurements for samples containing smaller or diluted samples due to diminished light scattering intensity (Gigault and Hackley 2013; Loeschner et al. 2013). As an alternative, empirical size calibration using the retention time of size standards is widely applied in the AF4 (Mudalige et al. 2015b). In this case, well-characterized size standards are essential, but their availability is limited. In the past, only the National Institute of Standard and Technology (NIST) traceable polystyrene spheres' standard reference materials (SRM) were available. NIST recently introduced gold nanoparticles and silver nanoparticles SRM as size standards. Due to stability against aggregation and durability in the storage, the application of polystyrene size standards for the size calibration in the analysis of various nanomaterials is still a common practice.

In AF4 experiments, the retention time of a given particle is dependent upon cross flow-to-channel flow ratio, diffusion coefficient of particle, and membrane-particle interactions (Du and Schimpf 2002; Litzen and Wahlund 1991; Ulrich et al. 2012). For example, Gigault and coworkers studied size-independent influence of the material-specific properties of nanoparticles on their retention behavior in the AF4 by comparing four different kinds of nanoparticle populations with identical nominal size (Gigault and Hackley 2013). Their findings summarize that the membrane-particle interaction is the main reason for the size-independent material-specific retention in the AF4. Bedizen and coworkers studied the membrane-particle interaction of titanium dioxide with varying the membrane-type and zeta potential of the particle by means of changing the running media composition (Bendixen et al. 2014). As a summary of the study, zeta potential itself does not predict the retention behavior of  $\text{TiO}_2$  nanoparticles and forces other than the electrostatic repulsion play an important role on the retention (Bendixen et al. 2014).

Here, we report and explain the differences observed in the retention time of gold nanoparticles and polystyrene size standards with different properties (i.e., material, surface coating, running media composition, and membrane). We tested the applicability of polystyrene particles, as calibration standards for Au NPs having various surface coatings and as a result, and we calculated the deviations associated with the size measurement due to the standard mismatch in the empirical size calibration. In all the cases, DLVO theory and the effects of diffusion have been used to explain the observed variable retention.

## Experimental section

### Materials and reagents

Type I ultrapure water ( $18.2 \text{ M}\Omega \text{ cm}$ ), obtained from an EMD Millipore water purification system (Model No: Direct-Q 3UV, Billerica, MA, USA), was utilized for all solution preparations. Sodium 3-mercapto-1-propane-sulfonate, and bis(p-sulfonatophenyl) phenylphosphine (phosphine), was purchased from Sigma-Aldrich (Saint Louis, MO, USA). Sodium citrate was purchased from Fisher Scientific (Houston, TX, USA). Au NPs reference materials with nominal diameters of 10 (RM8010),

30 (RM8012), and 60 (RM8013) nm were purchased from the National Institute of Standards and Technology (NIST, Gaithersburg, MD). NIST traceable nanosphere polystyrene nanoparticle standards with nominal diameter of 20 (3020A), 40 (3040A) 80 (3080A), and 100 (3010A) nm were purchased from Fisher Scientific. Millipore precut regenerated cellulose membranes with a molecular weight cutoff of 30 kDa (30kDaMC) and polyethylene sulfone (PES) membranes with a molecular weight cutoff of 30 kDa (30kDaPES) were purchased from Wyatt Technology (Santa Barbara, CA, USA). Amicon Ultra 0.5 ml centrifugal filter units with a molecular weight cutoff of 3 kDa were purchased from EMD Millipore and used to remove excess phosphine. Disposable folded capillary cells and surface zeta potential accessory, from Malvern Instruments (Worcestershire, UK), were used for measuring particle zeta potential and measuring membrane surface zeta potential, respectively.

#### Gold nanoparticle functionalization

Phosphine-coated Au NP suspensions were prepared by mixing citrate-stabilized Au NP reference materials with the required amount of phosphine to keep the phosphine concentration constant, at 0.5 mg/mL. After the phosphine was added, the solutions were vortexed at room temperature for 2 min to assist with the exchange of citrate molecules with phosphine. Phosphine-coated Au NPs were used directly for AF4 analysis. Sodium 3-mercapto-1-propanesulfonate-functionalized Au NPs were prepared mixing 10  $\mu$ M solution of thiol compound dropwise to Au NPs and were vortexed between additions of each drop. The functionalized particles were isolated by centrifugation, using 3 kDa molecular weight cutoff centrifugal filter units and subsequently suspended in the appropriate solvent.

#### Determination of particle and membrane zeta potential

Particle zeta potential measurements were performed using a Möbiu $\zeta$  system (Wyatt Technology). Samples for the zeta potential measurements were prepared by diluting the Au NPs solutions with a sodium citrate to match the ionic strength and composition of the AF4 carrier fluid. Measurements were performed using a Möbiu $\zeta$  Dip Cell, whereas the membrane zeta

potential was assessed using a Zetasizer Nano ZS (Malvern Instruments, UK). A detailed description of the membrane zeta potential measurement technique is available in our previous publication (Mudalige et al. 2015c). Briefly, membrane samples were cut into rectangles to an approximate size of 5 mm by 4 mm and pasted onto the replaceable sample holder of the Malvern surface cell accessory. A small amount of a high-viscosity nail polish was used as glue to prevent the liquid from soaking onto the membrane. Thermo Scientific NIST traceable, water-soluble, polystyrene particle size standards (100 nm cat # 3100A) were used as tracer particles, and the original suspension media of the particles were replaced with the appropriate electrolyte by centrifugation and suspension of the particle pellets. The sample holder with the glued membrane was screw-fitted in the cell. Sample height was adjusted with a cell height adjustment tool. The sample fitted on the cell was washed with water followed by the tracer particle electrolyte solution. The cell was placed in a cuvette with the tracer particles and equilibrated for 1 h. The zero displacement sample position was adjusted with the count rate meter of the Malvern Zetasizer system. The zeta potential of the tracer particles was measured in triplicate at four different displacement values, using increments of 125 microns. On the other hand, the zeta potential of the particles without any effect from the membrane was measured using a very large displacement value of 1000 microns. The displacement of the membrane was plotted against the tracer particle zeta potential, and the membrane zeta potential was calculated by subtracting the y intercept from the free tracer particle zeta potential (Figures S1–S6) (Mudalige et al. 2015c).

#### Nanoparticle separation by AF4

A Wyatt Technology (Santa Barbara, CA) short channel Eclipse 3 AF4 system composed of a flow control unit and channel compartment (short channel with 145 mm length and 350 micron spacer) was coupled to an Agilent Technologies (Santa Clara, CA) 1200 high-performance liquid chromatography (HPLC) system, which contains a pump (G1311B), auto-sampler (G1329B), and UV-visible detector (G1315D). A polyvinylidene difluoride (PVDF) hydrophilic 0.1 micron membrane filter (EMD Millipore, Billerica, MA) was used just after the pump. The

pump was used to control liquid flow into the channel compartment, and an auto-sampler was used for sample introduction.

Precut membranes were soaked overnight in 20 % isopropanol, washed with Type I ultrapure water and equilibrated with carrier fluid inside the AF4 channel for 1 h. Fifty microliter of sample (concentrations at 5 ppm for each size fraction of Au NPs and 10 ppm of PS NPs) was analyzed during each run using the conditions listed in Table 1, and each measurements was conducted in triplicate. The absorbance signal was collected at a wavelength of 520 nm using a 10 nm bandwidth with respect to the 890 nm (20 nm) reference peak for gold nanoparticles and 254 nm using a 20 nm bandwidth with respect to the 890 nm (20 nm) reference peak for PS NPs.

## Results and discussion

### Determination of particle and membrane zeta potential

The zeta potential and size of the studied standard nanoparticles and the membranes used in the AF4 experiments in the presence of citrate electrolyte were assessed before each experiment (Table 2). In the specific case of the studied nanoparticle standards, the measurements reveal that all were negatively charged at the studied conditions, likely due to the deprotonation of the functional groups in the surface capping (citrate, phosphine, thiol, and carboxyl groups) of the nanoparticles at the studied pH (8.1) of the carrier fluid (citrate electrolyte). Moreover, compression of the electrical double layer (EDL) with an increase in the ionic strength of the electrolyte resulted in a slight decrease in the zeta potential of both particles and

membranes (Elimelech et al. 1995). Between 0.1 and 1 mM citrate electrolyte, more important variations in the zeta potential values are observed for 30-nm Au NPs capped with phosphine (i.e., zeta potential varies between  $-112$  and  $-73.5$  mV), as compared with 10-nm Au NPs capped with citrate (where zeta potential only varies between  $-91.7$  and  $-87.2$  mV). This observation can be explained by the increase in adsorbed citrate ion density on the surface of the particles due to the presence of excess citrate at elevated concentrations. The observed variations in the zeta potential of surface-modified nanoparticles as a function of electrolyte concentration are commonly associated with the properties of the capping ligands at the particle surface (Hotze et al. 2010). In the particular case of the membranes used, the increase in electrolyte concentration has a screening effect in the zeta potential, while on the membrane from regenerated cellulose the decrease in zeta potential is more prominent (Sze et al. 2003) as compared to the PES membrane (i.e., on the order of  $-68$  to  $-26.6$  mV for cellulose, and between  $-95.4$  and  $-79.5$  mV for PES membrane. The negative charge on the membrane is generated by ionization of the functional group on the membrane or/and adsorption of anions. The adsorptions of anions are more common in hydrophobic membranes (Ariza and Benavente 2001; Salg n et al. 2013). The large negative zeta potential for PES membrane for all three electrolyte concentrations can be explained based on the same phenomenon.

### AF4 analysis of polystyrene and functionalized gold nanoparticles

In this study, we evaluated the applicability of PS NPs as calibration standards for the size measurement of Au NPs having different surface functionalities. Size-

**Table 1** AF4 analysis parameters

Step	Designation	Time(min)	Flow(mL/min)
1	Elution	0.00–1.0	Channel flow 0.5, cross flow 0.0
2	Focus	1.0–2.0	Channel flow 0.5, cross low 1.0
3	Focus + injection	2.0–5.0	Channel flow 0.5, cross flow 1.0, injection flow 0.2 mL min
4	Focus	5.0–8.0	Channel flow 0.5, cross flow 1.0
5	Elution	8.0–120	Channel flow 0.5, cross flow 1.0
6	Elution	120.0–125.0	Channel flow 0.5, cross flow 0.0

**Table 2** Summary of zeta potential measurements under different electrolyte concentrations at pH 8.1

Particle/surface coating		Zeta potential (mV)		
		0.1 mM citrate	0.5 mM citrate	1.0 mM citrate
1.	10 nm/citrate/Au	$-91.7 \pm 4.4$	$-88.0 \pm 3.3$	$-87.2 \pm 2.1$
2.	30 nm/citrate/Au	$-106.1 \pm 0.3$	$-88.7 \pm 1.8$	$-85.7 \pm 1.0$
3.	60 nm/citrate/Au	$-112.1 \pm 4.7$	$-91.9 \pm 2.6$	$-91.5 \pm 0.2$
4.	10 nm/phosphine/Au	$-87.6 \pm 3.6$	$-76.5 \pm 0.5$	$-76.4 \pm 1.0$
5.	30 nm/phosphine/Au	$-119.6 \pm 0.1$	$-87.4 \pm 3.8$	$-79.9 \pm 0.6$
6.	60 nm/phosphine/Au	$-124.0 \pm 2.7$	$-92.1 \pm 1.4$	$-89.1 \pm 1.2$
7.	10 nm/thiol/Au	$-89.2 \pm 0.9$	$-84.9 \pm 3.9$	$-80.0 \pm 4.8$
8.	30 nm/thiol/Au	$-110.1 \pm 1.8$	$-85.8 \pm 2.6$	$-81.9 \pm 1.2$
9.	60 nm/thiol/Au	$-110.3 \pm 3.3$	$-89.2 \pm 2.2$	$-88.0 \pm 0.7$
10.	20 nm/PS	$-76.0 \pm 3.7$	$-69.4 \pm 4.2$	$-66.1 \pm 4.7$
11.	40 nm/PS	$-71.4 \pm 2.7$	$-68.9 \pm 1.7$	$-65.9 \pm 0.8$
12.	80 nm/PS	$-98.5 \pm 1.4$	$-83.2 \pm 2.0$	$-80.1 \pm 1.4$
13.	100 nm/PS	$-102.2 \pm 2.9$	$-92.4 \pm 9.1$	$-91.8 \pm 0.9$
14.	Cellulose membrane	$-68.0 \pm 1.2$	$-33.8 \pm 2.3$	$-26.6 \pm 1.9$
15.	PES membrane	$-95.4 \pm 4.5$	$-84.8 \pm 3.8$	$-79.5 \pm 2.9$

based calibration curves were made for both kinds of nanoparticles having various surface coatings. Here, we used sodium citrate solutions of varying concentrations at pH 8.1 as working fluid for all the experiments, due to the instability of citrate-coated gold nanoparticles in other electrolytes. Citrate ions physisorbed on the hydrophobic gold surface provide colloidal stability in aqueous suspensions (Lin et al. 2004). A phosphine compound bearing sulfonate group at the end of benzene ring was also used as a stabilizing agent and the phosphine chemisorbed on to the gold surface making a more stable coating (Lin et al. 2004; Westermark et al. 1999). Sodium 3-mercaptopropylsulfonate-functionalized gold nanoparticles were also used, since thiol forms a covalent bond on the gold surface making it a very stable coating (Hakkinen 2012).

Size-based retention of the functionalized Au and PS NPs onto a 30-kDa regenerated cellulose membrane at different electrolyte concentrations is shown in Fig. 1. Phosphine-coated gold nanoparticles were unable to recover at 1.0 mM citrate concentration due to membrane fouling, and therefore, these experiments are not shown in the figure. Although we generally observe increased retention time of Au and PS NPs with increasing nominal size and salt concentrations, the effect is dependent on the surface functional group. For instance, in Fig. 1a, at the lowest electrolyte

concentration (0.1 mM sodium citrate), the retention time for 10-nm Au NPs is comparable for all the surface functionalities (citrate, phosphine, and thiol groups), and more important differences are observed as the nominal size increases (60 nm). Here, we did not observe any correlation between zeta potential and retention time of nanoparticles. For example, phosphine-coated nanoparticles having the highest negative zeta potential should equilibrate far away from the barrier membrane and must have the shortest retention time. We observed the longest retention time for the phosphine-coated particles. In this case, contribution from membrane-particle interaction other than electrostatic repulsion may play a critical role. Various forms of membrane-particle interactions such as van der Waals, dipole-dipole, and hydrophobic interactions were described in recent literature (Du and Schimpf 2002; Ulrich et al. 2012). Due to the nature of the surface coating material, the polar group of each molecule, hydrophobicity, and polarizability may play a critical role in the membrane-particle interaction causing variable retention time.

In the case of polyethylene sulfone membranes, prolonged retention times were observed for all forms of particles despite having a much higher zeta potential of the membrane compared with surface zeta potential of cellulose membrane (Fig. 2). Prolonged retention times indicate the relatively strong

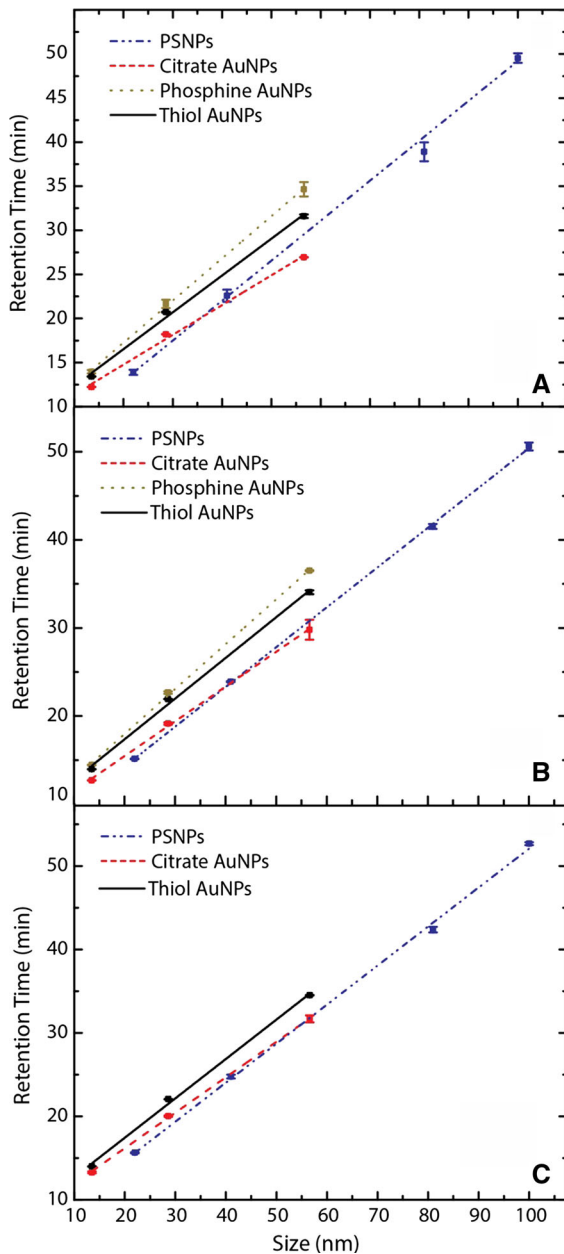


**Fig. 1** Size-based retention of polystyrene (*dash dotted*) with citrate (*dash*), phosphine (*dotted*), and thiol-functionalized gold nanoparticles (*solid*) showing material and surface coating specificity at citrate running media concentrations of 0.1 mM (**a**), 0.5 mM (**b**), and 1.0 mM (**c**) on a 30-kDa regenerated cellulose membrane

attractive forces with respect to electrostatic repulsion between particles and membrane. We also observed longer retention time for sodium 3-mercapto-1-propanesulfonate-functionalized Au NPs compared

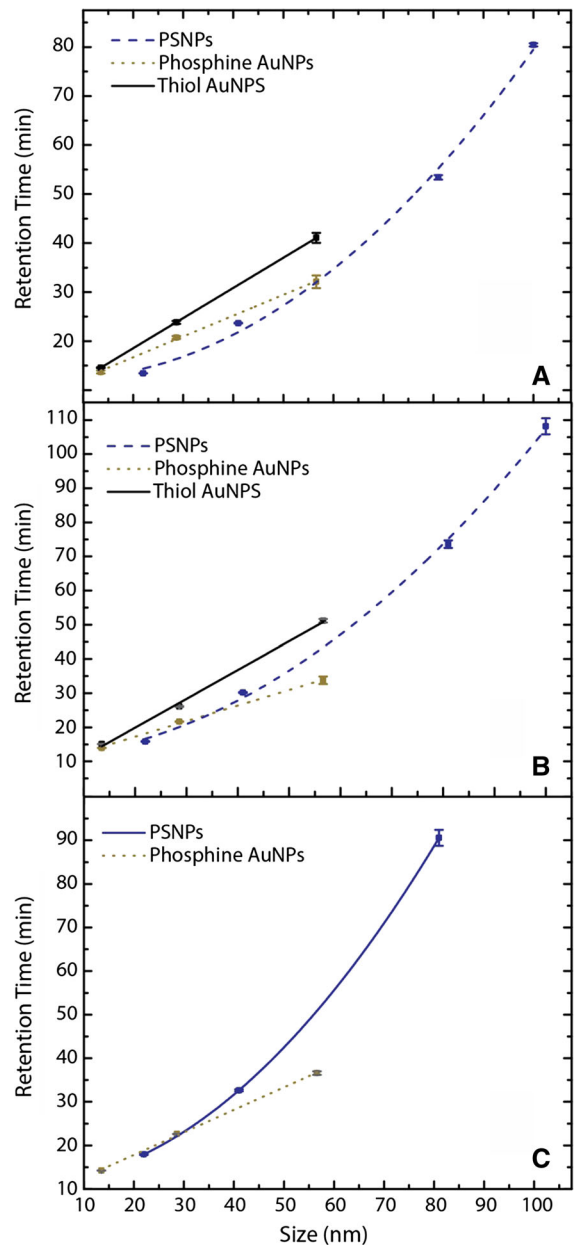


**Fig. 2** Size-based retention of polystyrene (*dash dotted*) with phosphine (*dotted*), and thiol-functionalized gold nanoparticles (*solid*) showing material and surface coating specificity at citrate running media concentrations of 0.1 mM (**a**), 0.5 mM (**b**), and 1.0 mM (**c**) on a 30-kDa polyethylene sulfone membrane

with bis(*p*-sulfonatophenyl) phenylphosphine-functionalized Au NPs, which is the opposite of the elution order observed with the application of cellulose membrane. A nonlinear retention was observed only for the polystyrene particles on PES membranes. In

this case, larger particles which equilibrate closer to the membrane exhibited longer retention time than expected. This observation can be attributed to the membrane–particle distance-dependent interactions. In the application of polystyrene, particles for calibration may generate completely misleading size calculations.

As previously mentioned, the observed differences in retention time for this set of experiments are dependent upon cross flow-to-channel flow ratio, diffusion coefficient of particle, and membrane–particle interactions. Although within all the experiments, the cross flow was maintained constant ( $8.1 \times 10^{-6}$  m/s), cross flow drags the particles toward the membrane. Diffusion ( $D_0$ , which is inversely proportional to the particle size) will push particles away from the membrane (Table 3). The third factor influencing retention time is the membrane–particle interaction. The total strength of these forces depends on the membrane–particle equilibrium distance, which is determined by particle size, indicating that membrane–particle interactions are also size dependent. To better understand the differences in the retention time observed here, classical DLVO theory is used here to estimate the NPs–membrane surface interaction profiles for the experiments conducted in sodium citrate electrolyte (Petosa et al. 2010). Classical DLVO theory considers the sum of London van der Waals

attraction, and electrical double-layer repulsion forces result in the calculation of the total interaction energy ( $\Phi_{Total}$ ). Here the total interaction forces have been determined by considering the NP–membrane system as a sphere–plate interaction (Petosa et al. 2010). Calculated Hamaker constants of  $2.68 \times 10^{-19}$  J (Au NPs–water–cellulose),  $2.0 \times 10^{-19}$  J (Au NPs–water–PES),  $4.26 \times 10^{-20}$  J (polystyrene NPs–water–cellulose), and  $3.18 \times 10^{-19}$  J (polystyrene NPs–water–PES) are used for all the studied systems. Values of the key parameter from the calculated total interaction energy profiles, namely the maximum height of the repulsive energy barrier ( $\Phi_{max}$ ), are reported in Table 3, and DLVO profiles for membrane–particle interactions are reported in supporting information (Figure S5–S8). As observed in the table, for each particle  $\Phi_{max}$  decreases in height with increase in the concentration of sodium citrate for all the cases. This observation is in consistency with the results conducted in the AF4 (supporting information Figures S5–S8).

This study was performed to demonstrate the importance of calibration standard matching for an accurate size determination in the AF4 and to demonstrate the magnitude of error associated with the mismatching of calibration standards. For a better comparison, we calculated the expected size of gold nanoparticle using polystyrene nanoparticles as size

**Table 3** Summary of experiments conducted under different electrolyte concentrations at pH 8.1

Particle/surface	$D_0$ ( $10^{-11}$ m <sup>2</sup> /s)	Membrane					
		0.1 mM citrate		0.5 mM citrate		1.0 mM citrate	
		$\phi_{max}$ (k T)		$\phi_{max}$ (k T)		$\phi_{max}$ (k T)	
		Cellulose	PES	Cellulose	PES	Cellulose	PES
1. 10 nm/citrate/Au	4.25	31	46	2	25	0	15
2. 30 nm/citrate/Au	1.42	73	109	4	54	0	31
3. 60 nm/citrate/Au	0.71	150	224	10	110	0	68
4. 10 nm/phosphine/Au	4.25	25	39	0	18	0	11
5. 30 nm/phosphine/Au	1.42	73	110	2	47	0	21
6. 60 nm/phosphine/Au	0.71	152	229	5	99	0	56
7. 10 nm/thiol/Au	4.25	29	44	1	22	0	12
8. 30 nm/thiol/Au	1.42	72	109	2	48	0	25
9. 60 nm/thiol/Au	0.71	143	216	5	100	0	57
10. 20 nm/PS	2.13	66	90	21	65	10	52
11. 40 nm/PS	1.06	117	159	38	120	18	97
12. 80 nm/PS	0.53	295	399	93	279	47	232
13. 100 nm/PS	0.43	373	504	126	374	68	321























standards in each citrate concentration with both cellulose and PES membranes. Here, we used linear regression equations to calculate the retention time of 25.0-nm and 50.0-nm polystyrene particles in particular experimental conditions. The actual size of Au NPs at comparable retention times was calculated using a regression equation for Au NPs. Data for this are shown in Table 4, which include proportional sizes of nanoparticles clearly indicating the size deviation from the expected values.

## Conclusion

We have studied the effect of material-specific membrane–particle interaction on the retention times of nanoparticles in asymmetric flow field-flow fractionation by varying the membrane type, particle coating, and the electrolyte concentrations. As expected, particle zeta potential decreased with the

increase in the electrolyte concentrations and the same trend was followed for the surface zeta potential of a regenerated cellulose membrane. In the case of the PES membrane, zeta potential remains almost the same with the increase in citrate concentration, possibly due to the increase in adsorption of citrate molecules. We did not observe any consistent correlation between the zeta potential and the retention time in the analysis of functionalized Au NPs and polystyrene nanoparticles; therefore, non-electrostatic interactions play a vital part of the membrane–particle interactions (Ulrich et al. 2012). We observed linear relationships between particle size and retention time for all of the experimental conditions, except for the PS nanoparticles with PES membrane. In this case, both particle and membrane are hydrophobic organic polymers having somewhat similar properties and the nonlinearity is caused by longer retention of the larger particles due to the distance-dependent membrane–particle interactions. Most importantly, we calculated

**Table 4** Actual size of gold nanoparticles having equivalent retention times of 25.0- and 50.0-nm polystyrene particles at various analytical conditions

particle type	0.1 mM citrate as running media			0.5 mM citrate as running media			1.0 mM citrate as running media		
	Equation	For 25.0 nm	For 50.0 nm	Equation	For 25.0 nm	For 50.0 nm	Equation	For 25.0 nm	For 50.0 nm
Styrene	$Y = 0.45X + 3.6$	 25.0	 50.0	$Y = 0.45X + 5.2$	 25.0	 50.0	$Y = 0.46X + 5.3$	 25.0	 50.0
Gold citrate	$Y = 0.33X + 8.01$	 21.4	 55.0	$Y = 0.39X + 7.6$	 22.7	 51.3	$Y = 0.42X + 7.7$	 22.0	 49.5
Gold phosphine	$Y = 0.48X + 7.7$	 15.8	 39.5	$Y = 0.51X + 7.8$	 17.2	 39.4	$Y = 0.47X + 8.0$	 19.1	 43.9
Gold thiol	$Y = 0.42X + 8.2$	 16.9	 44.0	$Y = 0.46X + 8.1$	 18.2	 42.6	x	x	x

Regression equations are indicated for each analytical condition. (For the comparison, nanoparticles are represented in proportional size)



the error associated with the application of the polystyrene standards for size calibration for gold nanoparticles having various surface functionalities and found that the error can be up to 33 %, depending on analysis condition and the size of the analyte. In conclusion, appropriate standards having an identical coating of the sample are necessary for the measurement of the unknown nanoparticles with empirical size calibration.

**Acknowledgments** These studies were conducted using the Nanotechnology Core Facility (NanoCore) located on the US Food and Drug Administration's Jefferson Laboratories campus (Jefferson, AR), which houses the FDA National Center for Toxicological Research and the FDA Office of Regulatory Affairs Arkansas Regional Laboratory. We thank Dr. Marilyn Khanna, Crystal Ford, Dr. Venu Gopal Bairi, Dr. Jin-hee Lim, and Dr. Yasith Nanayakkara for their support and valuable comments on the draft manuscript. The views expressed in this document are those of the researchers and should not be interpreted as the official opinion or policy of the US Food and Drug Administration, Department of Health and Human Services, or any other agency or component of the US Government. The mention of trade names, commercial products, or organizations is for clarification of the methods used and should not be interpreted as an endorsement of a product or manufacturer.

## References

- Ariza MJ, Benavente J (2001) Streaming potential along the surface of polysulfone membranes: a comparative study between two different experimental systems and determination of electrokinetic and adsorption parameters. *J Membrane Sci* 190:119–132
- Bendixen N, Losert S, Adhart C, Lattuada M, Ulrich A (2014) Membrane–particle interactions in an asymmetric flow field flow fractionation channel studied with titanium dioxide nanoparticles. *J Chromatogr A* 1334:92–100
- Chithrani BD, Ghazani AA, Chan WCW (2006) Determining the size and shape dependence of gold nanoparticle uptake into mammalian cells. *Nano Lett* 6:662–668. doi:[10.1021/nl052396o](https://doi.org/10.1021/nl052396o)
- De M, Ghosh PS, Rotello VM (2008) Applications of nanoparticles in biology. *Adv Mater* 20:4225–4241
- Du Q, Schimpf ME (2002) Correction for particle-wall interactions in the separation of colloids by flow field-flow fractionation. *Anal Chem* 74:2478–2485
- Elimelech M, Gregory J, Jia X, Williams RA (1995) Particle deposition and aggregation—measurement, modelling and simulation. Elsevier, New York
- Gallego-Urrea JA, Tuoriniemi J, Hassellöv M (2011) Applications of particle-tracking analysis to the determination of size distributions and concentrations of nanoparticles in environmental, biological and food samples TrAC. *Trends Anal Chem* 30:473–483
- Gigault J, Hackley V (2013) Observation of size-independent effects in nanoparticle retention behavior during asymmetric-flow field-flow fractionation. *Anal Bioanal Chem* 405:6251–6258
- Hakkinen H (2012) The gold-sulfur interface at the nanoscale. *Nat Chem* 4:443–455
- Hotze EM, Phenrat T, Lowry GV (2010) Nanoparticle aggregation: challenges to understanding transport and reactivity in the environment. *J Environ Qual* 39:1909–1924
- Lewinski N, Colvin V, Drezek R (2008) Cytotoxicity of nanoparticles. *Small* 4:26–49
- Lin SY, Tsai YT, Chen CC, Lin CM, Chen Ch (2004) Two-step functionalization of neutral and positively charged thiols onto citrate-stabilized Au nanoparticles. *J Phys Chem B* 108:2134–2139
- Litzen A, Wahlund KG (1991) Effects of temperature, carrier composition and sample load in asymmetrical flow field-flow fractionation. *J Chromatogr A* 548:393–406
- Loeschner K et al (2013) Optimization and evaluation of asymmetric flow field-flow fractionation of silver nanoparticles. *J Chromatogr A* 1272:116–125
- Lopez-Serrano A, Olivas RM, Landaluze JS, Camara C (2014) Nanoparticles: a global vision. Characterization, separation, and quantification methods. Potential environmental and health impact. *Anal Methods* 6:38–56
- Mitrano DM, Barber A, Bednar A, Westerhoff P, Higgins CP, Ranville JF (2012) Silver nanoparticle characterization using single particle ICP-MS (SP-ICP-MS) and asymmetrical flow field flow fractionation ICP-MS (AF4-ICP-MS). *J Anal Atom Spectrom* 27:1131–1142
- Mudalige TK, Qu H, Linder SW (2015a) Asymmetric flow field flow fractionation hyphenated ICP-MS as an alternative to cloud point extraction for quantification of silver nanoparticles and silver speciation: application for nanoparticles with protein corona. *Anal Chem* 87:7395–7401
- Mudalige TK, Qu H, Linder SW (2015b) An improved methodology of asymmetric flow field flow fractionation hyphenated with inductively coupled mass spectrometry for the determination of size distribution of gold nanoparticles in dietary supplements. *J Chromatogr A* 1420:92–97
- Mudalige TK, Qu H, Sánchez-Pomales G, Sisco PN, Linder SW (2015c) Simple functionalization strategies for enhancing nanoparticle separation and recovery with asymmetric flow field flow fractionation. *Anal Chem* 87:1764–1772
- Petosa AR, Jaisi DP, Quevedo IR, Elimelech M, Tufenkji N (2010) Aggregation and deposition of engineered nanomaterials in aquatic environments: role of physicochemical interactions. *Environ Sci Technol* 44:6532–6549
- Qu H, Mudalige TK, Linder SW (2014) Capillary electrophoresis/inductively-coupled plasma-mass spectrometry: development and optimization of a high resolution analytical tool for the size-based characterization of nanomaterials in dietary supplements. *Anal Chem* 86:11620–11627
- Salgyn S, Salgyn U, Soyer N (2013) Streaming potential measurements of polyethersulfone ultrafiltration membranes to determine salt effects on membrane zeta potential. *Int J Electrochem Sc* 8:4073–4084
- Sozer N, Kokini JL (2009) Nanotechnology and its applications in the food sector. *Trends Biotechnol* 27:82–89

- Sze A, Erickson D, Ren L, Li D (2003) Zeta-potential measurement using the Smoluchowski equation and the slope of the current-time relationship in electroosmotic flow. *J Colloid Interf Sci* 261:402–410
- Ulrich A et al (2012) Critical aspects of sample handling for direct nanoparticle analysis and analytical challenges using asymmetric field flow fractionation in a multi-detector approach. *J Anal Atom Spectrom* 27:1120–1130
- Wahlund KG (2013) Flow field-flow fractionation: critical overview. *J Chromatogr A* 1287:97–112
- Westermark G, Kariis H, Persson I, Liedberg B (1999) An infrared study on the chemisorption of tertiary phosphines on coinage and platinum group metal surfaces. *Colloid Surface A* 150:31–43